Electronic Supplementary Material (ESI) for Energy & Environmental Science.

Supplementary Information

Aeroelectrolyte for Atmospheric Open Electrochemical Cells

Yeji Lim[1], Yoon Jeong Yoo[1], Boran Kim[1], Suji Kim[1], Ga Yoon Kim[1], Won-Hee Ryu [1, *]

[1] Department of Chemical and Biological Engineering, Sookmyung Women's University, 100 Cheongpa-ro 47-gil, Yongsan-gu, Seoul, 04310, Republic of Korea

*Corresponding author

E-mail: whryu@sookmyung.ac.kr (Prof. Won-Hee Ryu)

Supplementary Figures

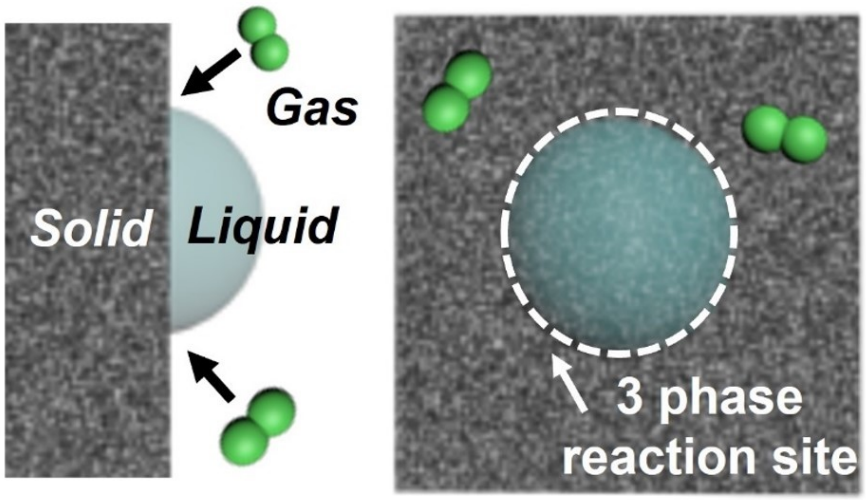

Fig. S1 Schematic illustration of the three-phase boundary.

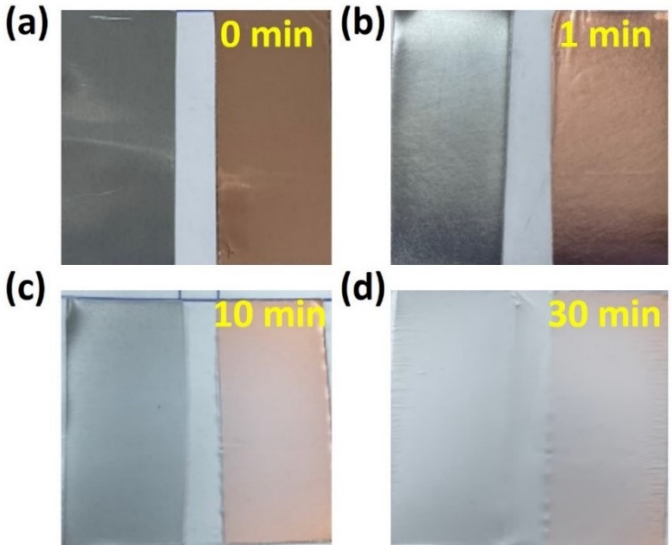

Fig. S2 Photographic images of electrodes coated with the salt bridge by varying the electrospinning time. Images of the salt bridge at electrospinning times of (a) 0 min, (b) 1 min, (c) 10 min and (d) 30 min.

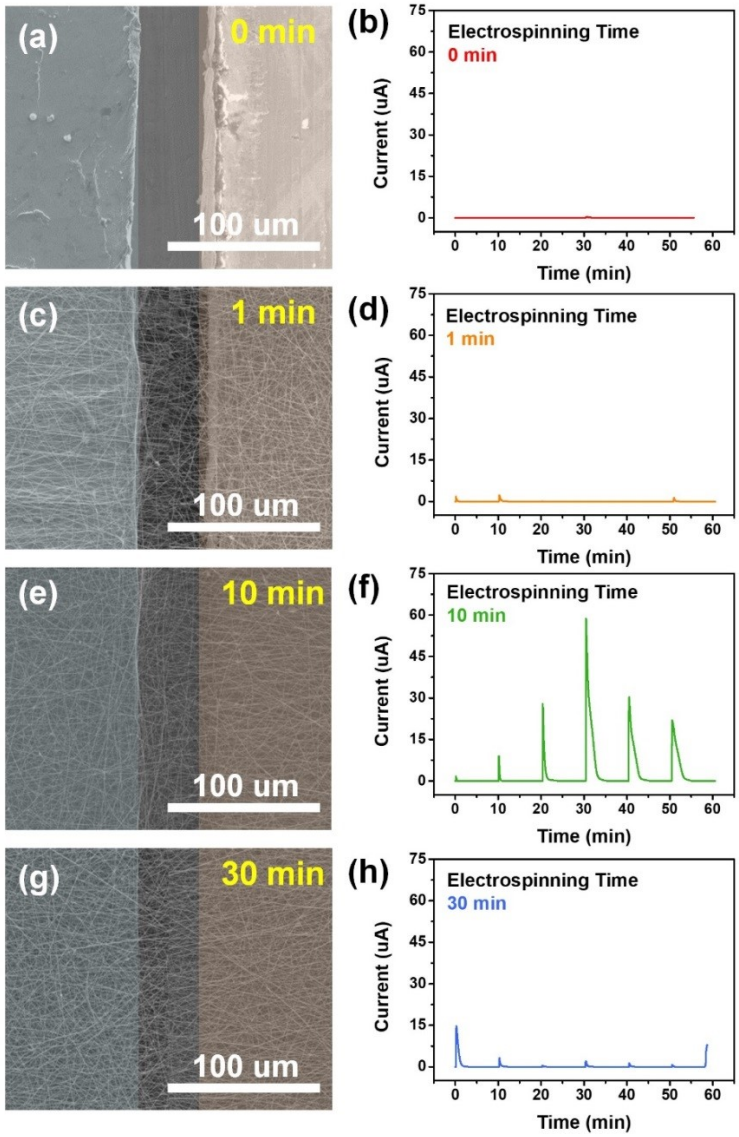

Fig. S3 SEM images captured of the salt bridge after various electrospinning times and the corresponding current measurements. SEM images of the electrodes during formation of the salt bridge taken at electrospinning times of (a) 0, (c) 1, (e) 10, and (g) 30 min. Corresponding results of the current test of the sprayed electrolyte cell with the salt bridge for electrospinning times of (b) 0, (d) 1, (f) 10, and (h) 30 min.

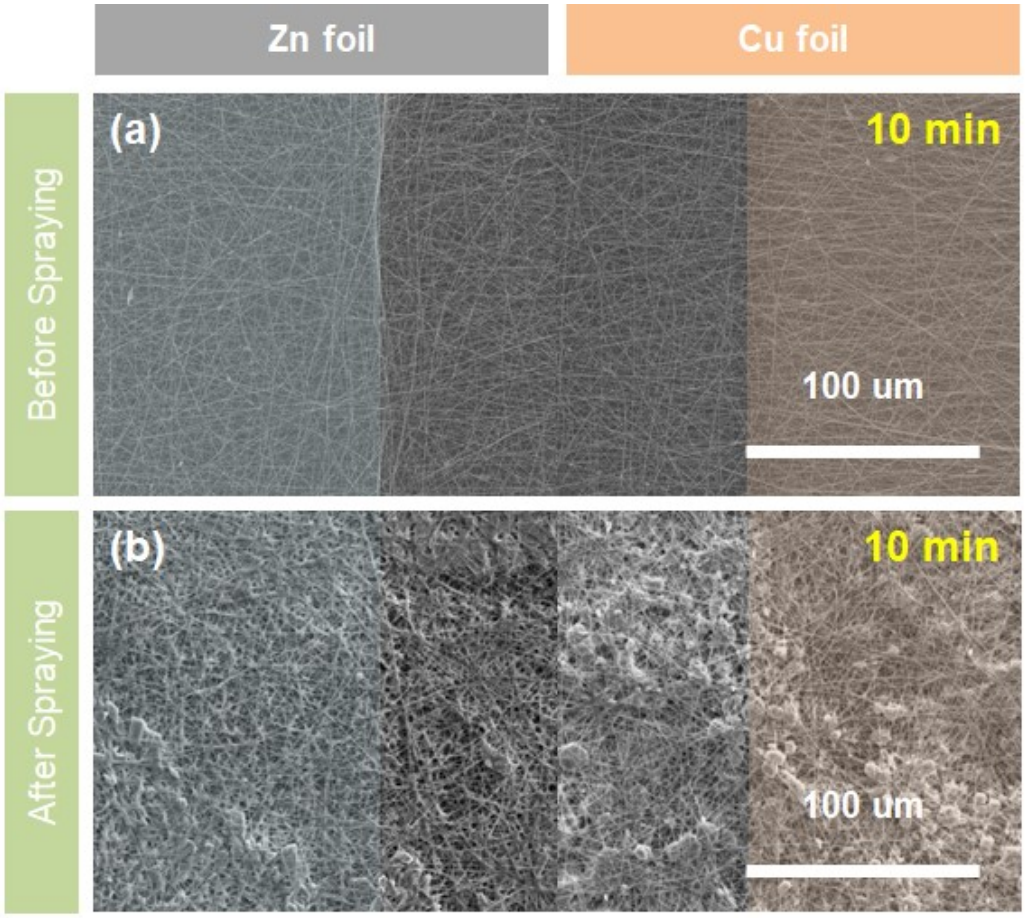

Fig. S4 Photographic images of electrodes coated with the salt bridge for 10 minutes of electrospinning time: (a) before applying sprayed electrolyte and (b) after applying electrolyte sprayed five times with a 10-minute interval.

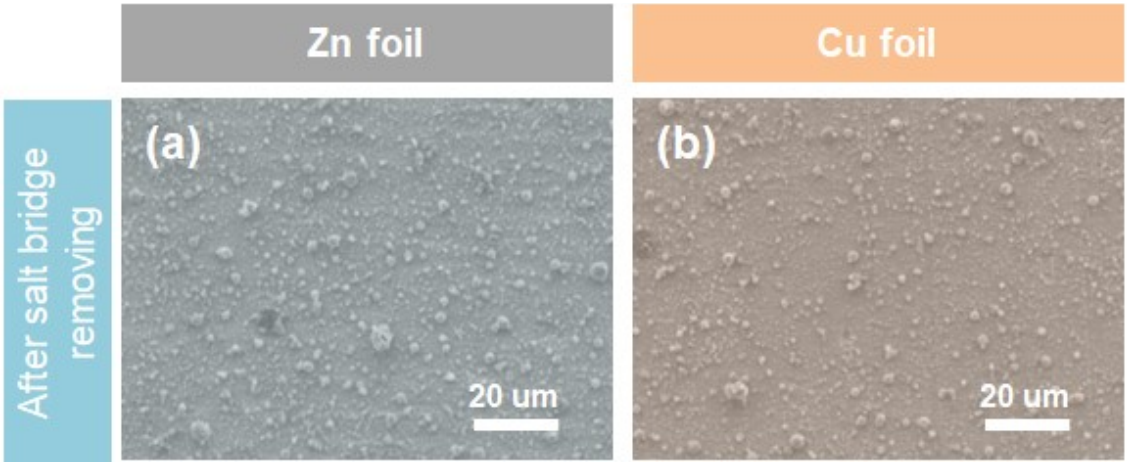

Fig. S5 Photographic images of electrodes without salt bridges, after applying electrolyte sprayed five times with a 10-minute interval.

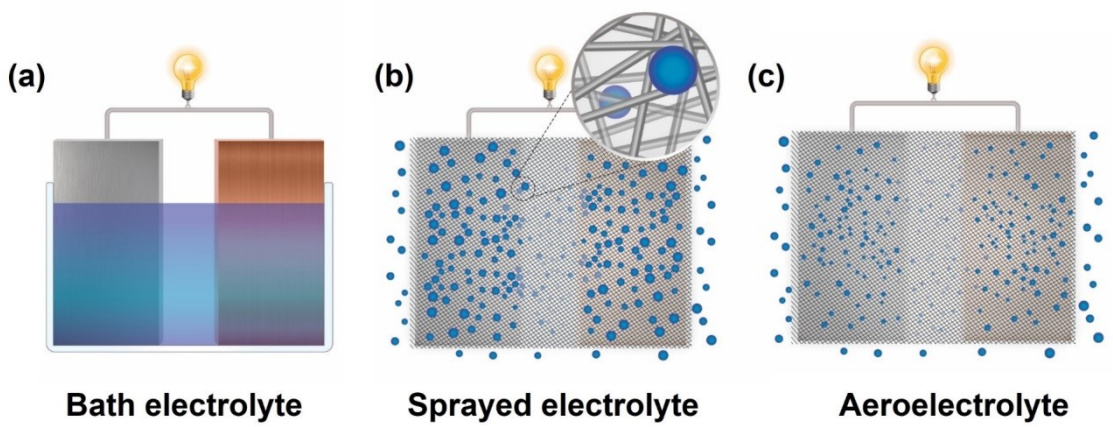

Fig. S6 Schematic images of the electrolyte cells with various electrolyte droplet sizes. Schematics of the (a) bath electrolyte system, (b) sprayed electrolyte cell with salt bridge, and (c) aeroelectrolyte system with salt bridge.

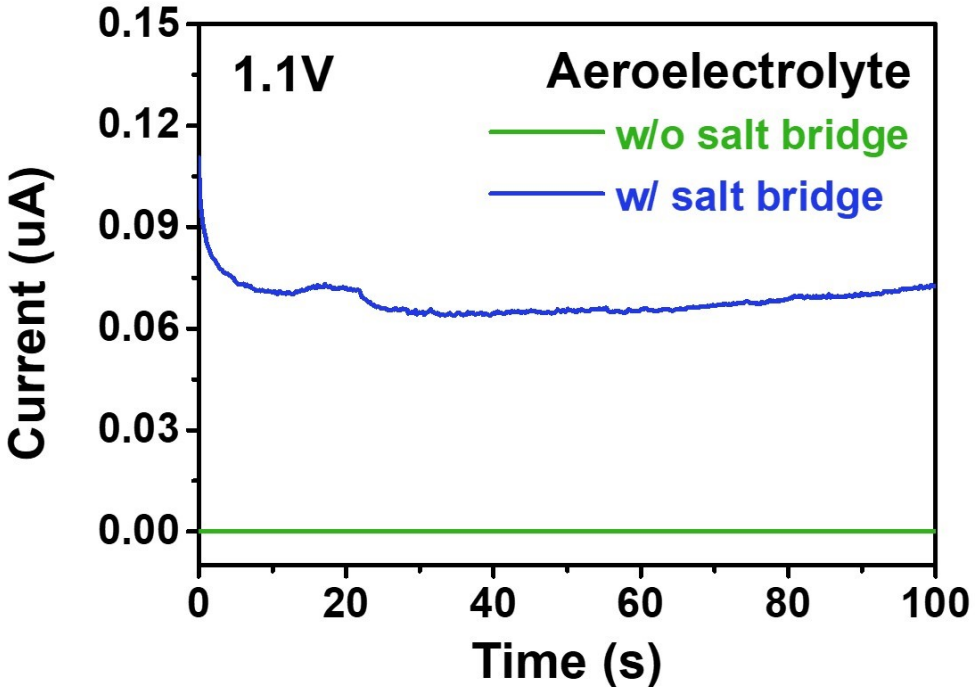

Fig. S7 Initial reaction kinetics and ion diffusivity of aeroelectrolyte system. Current produced by the aeroelectrolyte cells with/without salt bridges.

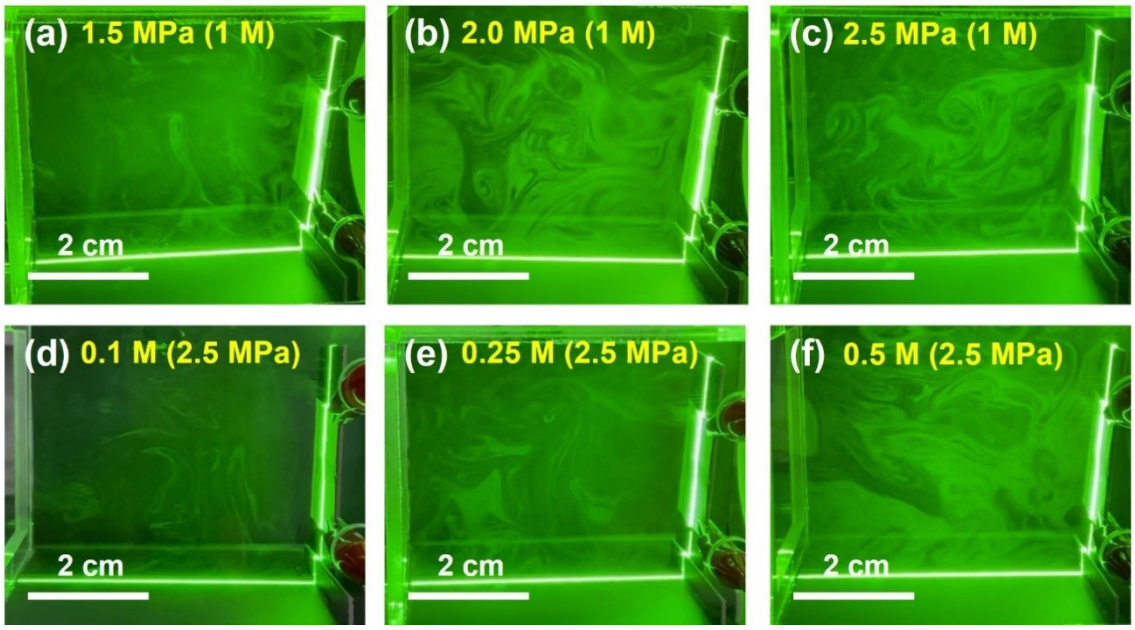

Fig. S8 Diffusion characteristics of the aeroelectrolyte at various aerosol generation pressures and $CuSO_4$ concentrations. Photographic images of the aeroelectrolyte with a generation pressure of (a) 1.5, (b) 2.0, and (c) 2.5 MPa with 1.0 M electrolyte. Photographic images of the aeroelectrolyte with an electrolyte concentration of (d) 0.1, (e) 0.25, and (f) 0.5 M at 2.5 MPa generation pressure.

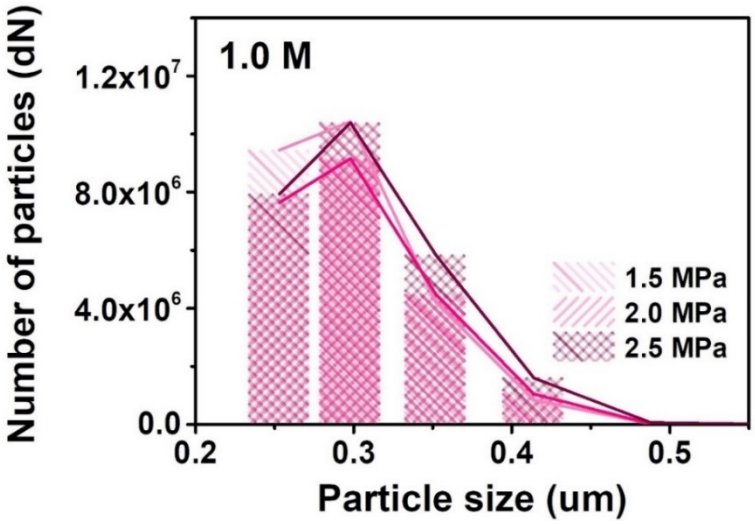

Fig. S9 Particle size distribution of the aeroelectrolyte generated at various pressures. Particle size distribution at 1.5, 2.0, and 2.5 MPa at a constant concentration of 1.0 M.

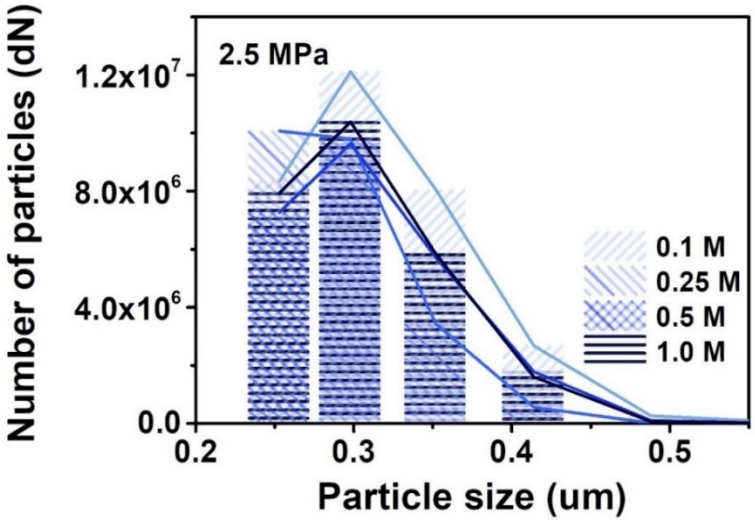

Fig. S10 Particle size distribution of the aeroelectrolyte for various electrolyte concentrations. Particle size distribution for the concentrations 0.1, 0.25, 0.5, and 1.0 M at 2.5 MPa.

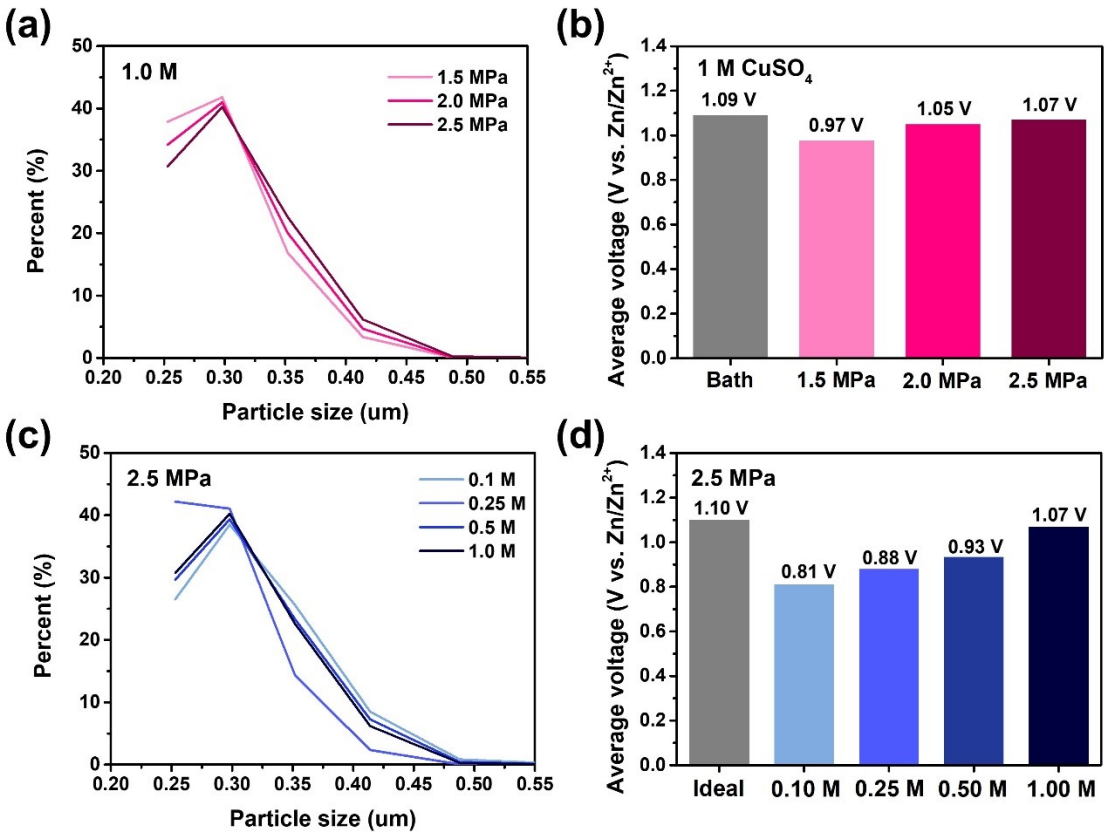

Fig. S11 Particle size fraction distribution of the aeroelectrolyte and average operating voltage of the aeroelectrolyte cell. Particle size distribution of the aeroelectrolyte under (a) pressure- and (c) concentration-controlled conditions. Average cell voltage values of the aeroelectrolyte cell under (b) pressure- and (d) concentration-controlled conditions.

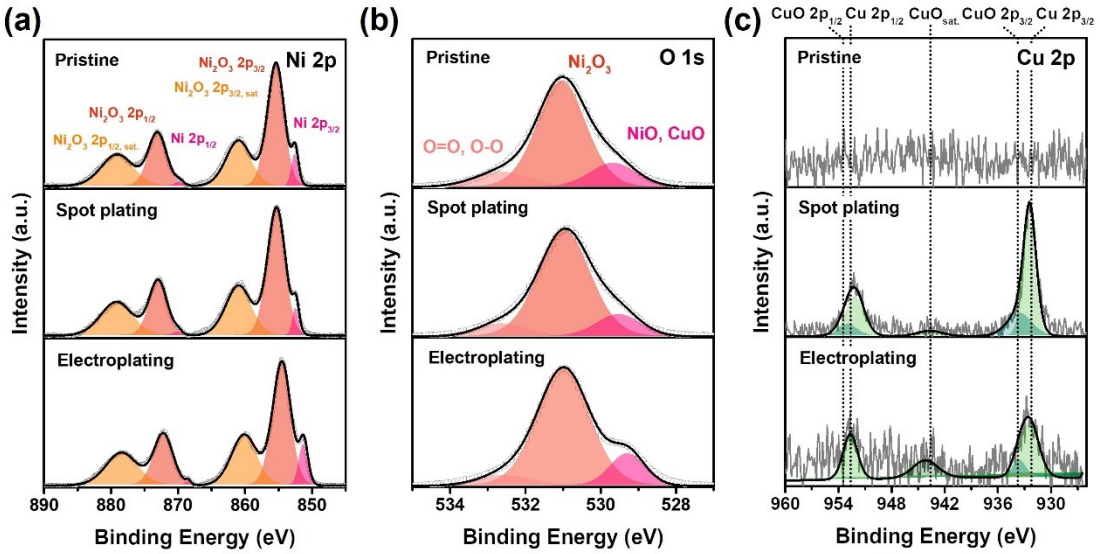

Fig. S12 *Ex-situ* analysis of Ni foil cathode. XPS results of (a) Ni 2p, (b) O 1s, and (c) Cu 2p obtained from pristine Ni foil, spot-plated Ni foil using the bath electrolyte, and electroplated Ni foil using the aeroelectrolyte.

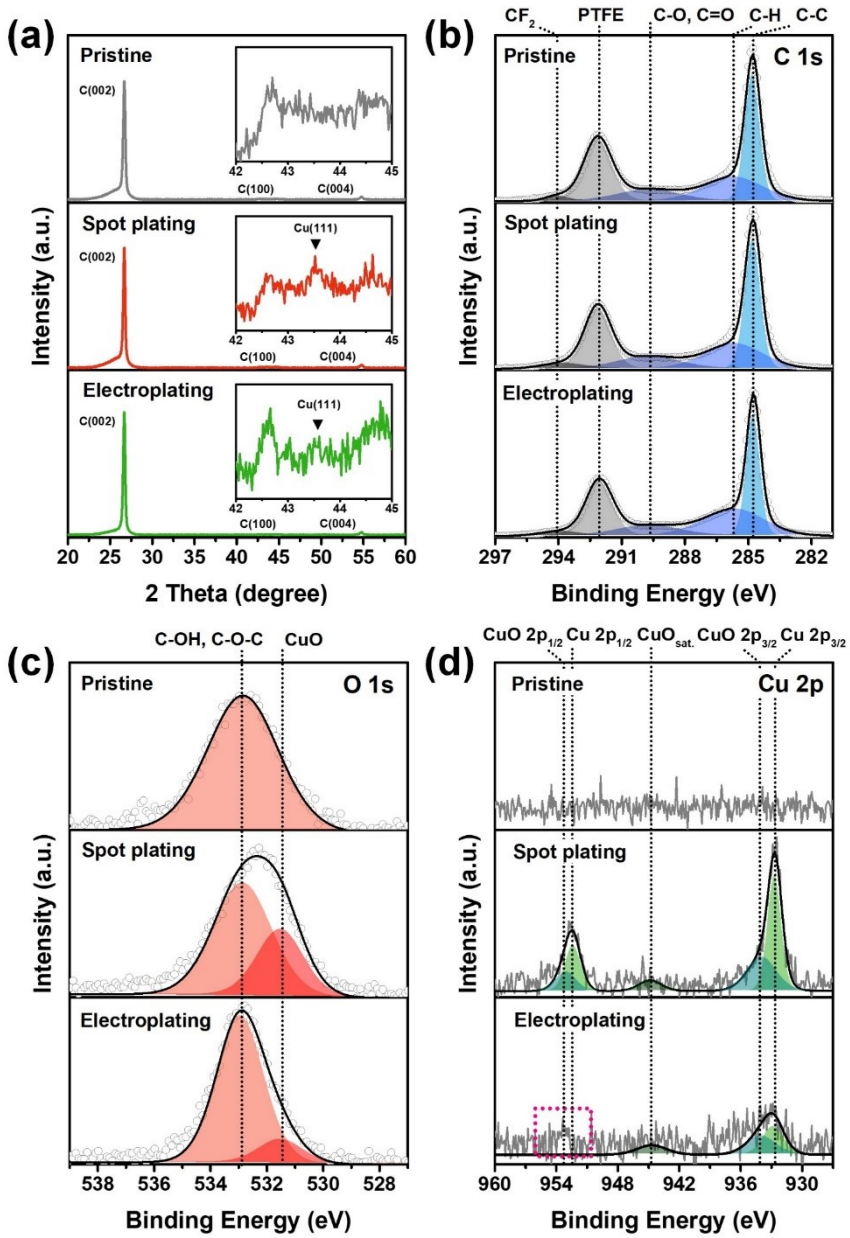

Fig. S13 *Ex-situ* analysis of carbon paper cathode. (a) XRD patterns of pristine carbon paper, spot-plated carbon paper using the bath electrolyte, and carbon paper electroplated using the aeroelectrolyte. XPS results of (b) C 1s, (c) O 1s, and (d) Cu 2p obtained from the pristine carbon paper, spot-plated carbon paper using the bath electrolyte, and electroplated carbon paper using the aeroelectrolyte.

Supplementary Videos

Video S1 Diffusion characteristics of aeroelectrolyte. High-speed camera video of the aeroelectrolyte generated at 2.5 MPa with 1 M electrolyte.

Supplementary Discussion

Relationship among the total contact area of the aerelectrolyte with the electrode surface, the amount of electrolyte generated, and the droplet diameter

Understanding the total contact area between the electrolyte and the electrode is crucial because the extent of the electrochemical reaction is proportional to the reaction area. Therefore, we established an equation to express the relationship among the total contact area of the aeroelectrolyte with the electrode surface, amount of electrolyte generated, and droplet diameter. Before formulating the equation, the following assumptions were made: (1) the total volume (V) of the aerosolized solution was assumed to be L, and consisted of a total of n particles with a constant size. (2) The radius (r) of individual aeroelectrolyte droplets is assumed to be constant across all the droplets. (3) All generated aeroelectrolyte droplets adhered to the electrode and were adsorbed in a perfect hemispherical shape with a radius of R. Based on assumptions (1) and (2), the following relationship can be established between the total amount of electrolyte consumed and the amount of aeroelectrolyte generated:

$$V = nV_r \tag{1}$$

$$L = n\frac{4}{3}\pi r^3 n \tag{2}$$

$$n = \frac{3L}{4\pi r^3} \tag{3}$$

Furthermore, based on assumption (3), the radius (R) of an adsorbed aeroelectrolyte droplet can be defined as follows:

$$V_r = V_R \tag{4}$$

$$\frac{4}{3}\pi r^3 = \frac{2}{3}\pi R^3 \tag{5}$$

$$R = 2^{2/3} r \tag{6}$$

Finally, by multiplying the total quantity of electrolyte by the adsorption area occupied by each droplet, the overall electrochemical reaction area was calculated as follows:

$$A_{total} = n\pi R^2 = \frac{3L}{2^{2/3} r} \tag{7}$$

***Ex-situ* analysis of Ni foil and carbon paper cathode**

The reaction mechanism and structural changes during the Daniell cell reaction were evaluated by subjecting the pristine, spot-plated, and electroplated cathode cells to *ex-situ* analysis. A spot-plated electrode was prepared using a bath electrolyte cell, and the electrochemical reaction was allowed to proceed for 1 s. The electroplated electrode was prepared by applying the aeroelectrolyte to the cell and allowing the electrochemical reaction to proceed for 2 h. All electrodes were washed with distilled water and dried before the experiment to remove the residual $CuSO_4$ salt. First, the Ni foil was analyzed using XPS after operating the Daniell cell with the aeroelectrolyte to confirm the chemical bonding on the electrode surface (**Fig. S10**). The Ni 2p spectra featured the same type of peak for all three the electrodes and the peak intensity did not change significantly. This observation confirms that the structure of the Ni foil remained relatively unchanged during both the spot plating and electroplating processes[1]. The peak at approximately 529 eV on the O 1s spectrum of the electroplated electrode intensified. However, this region was complicated by overlapping signals from NiO and CuO at 529.5 eV, making it difficult to precisely distinguish between the generated products[2]. On the other hand, the Cu 2p spectra clearly exhibited distinct peaks corresponding to Cu (at 952.48 and 932.4 eV) and CuO (at 953.5, 943.7, and 933.7 eV) for both the spot plated and electroplated samples, unlike the pristine electrode[2, 3]. The low peak intensities for both of the samples indicate that a small amount of Cu was formed through the electrochemical reactions. In addition, the electroplated sample had a lower signal-to-noise ratio, making it difficult to precisely differentiate the reaction products. However, the signals in the Cu and CuO regions were clearly distinguishable and supported the possibility of an electrochemical reaction with the aeroelectrolyte.

With respect to the Ni foil, the XRD and XPS results featured several overlapping peaks between Cu and Ni. Therefore, for a more accurate cross-validation, the same experiment was conducted by replacing the Ni foil with carbon paper (**Fig. S11**). On the XRD pattern, which was acquired to confirm the crystallinity of the electrode surface, the carbon peaks of all the electrodes had similar intensities and occurred at the same positions as those of the pristine electrode. This indicated that the carbon structure of all electrodes remained stable after the reaction. In contrast, unlike the pristine electrode, the peak corresponding to the Cu(111) plane at 43.5 ° was observed for the surfaces of the spot-plated and electroplated cathodes. This confirms that the Daniell cell reaction with the aeroelectrolyte occurred, as theoretically expected. The XPS profiles were recorded to confirm the chemical bonding on the electrode surface. On the C 1s spectra, the peak formation positions and intensities of the electrochemically reacted electrodes and pristine electrode were nearly identical[1, 4]. This indicates that the carbon surface underwent minimal chemical changes during the electrochemical reactions. However, on the O 1s spectra, unlike the pristine electrode,

a CuO bonding peak was observed at 531.5 eV for the surfaces of the spot plated and electroplated electrodes[2]. Although the peak intensity of the electroplated electrode is lower than that of the spot-plated electrode, a distinct peak was still observable[1]. Likewise, the Cu 2p spectra exhibited peaks corresponding to Cu (at 952.48 and 932.4 eV) and CuO (at 953.5, 943.7, and 933.7 eV) on the surfaces of the electrochemically reacted electrodes, unlike the pristine electrode[2, 3]. Similar to the O 1s spectra, smaller amounts of Cu and CuO were measured to exist on the electroplated electrode, but distinct signals were detected compared with the pristine electrode. These *ex-situ* data acquired after using the aeroelectrolyte cell demonstrate the feasibility of the Daniell cell reaction using aeroelectrolytes and further suggest the potential for electrochemical reactions utilizing aeroelectrolytes.

References

1. D. T. Tran, S. Prabhakaran, D. H. Kim, N. H. Kim and J. H. Lee, *Applied Catalysis B: Environmental*, 2021, **294**, 120263.
2. W. Kang, H. Guo and A. Varma, *Applied Catalysis B: Environmental*, 2019, **249**, 54-62.
3. S. Li, P. Ma, C. Gao, L. Liu, X. Wang, M. Shakouri, R. Chernikov, K. Wang, D. Liu and R. Ma, *Energy & Environmental Science*, 2022, **15**, 3004-3014.
4. F. Peng, Y. Lim, B. Kim, H.-S. Kim, Z. Li, Z. Zhou, J. Li and W.-H. Ryu, *Sustainable Materials and Technologies*, 2023, **35**, e00531.